REPORT DOCUMENTATION PAGE

Form Approved
OMB No. 0704-0188

1. REPORT DATE *(DD-MM-YYYY)*	2. REPORT TYPE	3. DATES COVERED *(From - To)*
10-08-2004	Journal Article	

4. TITLE AND SUBTITLE

Quantum and Quasi-classical Studies of the $O(^3P) + HCl \rightarrow OH + Cl(^2P)$ Reaction Using Benchmark Potential Surfaces (PREPRINT)

5a. CONTRACT NUMBER
F04611-03-C-0015

5b. GRANT NUMBER

5c. PROGRAM ELEMENT NUMBER

6. AUTHOR(S)
Tiao Xie and Joel Bowman (Emory Univ.); J.W. Duff and M. Braunstein (Spectral Sciences); B. Ramachandran (Louisiana Tech Univ.)

5d. PROJECT NUMBER
BMSB

5e. TASK NUMBER
R2FT

5f. WORK UNIT NUMBER

7. PERFORMING ORGANIZATION NAME(S) AND ADDRESS(ES)

Spectral Sciences Incorporated
4 Fourth Avenue
Burlington, MA 01803-3304

8. PERFORMING ORGANIZATION REPORT NUMBER

AFRL-PR-ED-TP-2004-268

9. SPONSORING / MONITORING AGENCY NAME(S) AND ADDRESS(ES)

Air Force Research Laboratory (AFMC)
AFRL/PRS
5 Pollux Drive
Edwards AFB CA 93524-7048

10. SPONSOR/MONITOR'S ACRONYM(S)

11. SPONSOR/MONITOR'S NUMBER(S)
AFRL-PR-ED-TP-2004-268

12. DISTRIBUTION / AVAILABILITY STATEMENT

Approved for public release; distribution unlimited

13. SUPPLEMENTARY NOTES
Submitted to the Journal of Chemical Physics.

14. ABSTRACT

We have performed quantum mechanical (QM) dynamics calculations within the independent-state approximation with new benchmark triplet A" and A' surfaces [B. Ramachandran *et al.* J. Chem. Phys. **119**, 9590 (2003).] for the ro-vibronic state-to-state measurements of the reaction $O(^3P) + HCl(v=2,j=1,6,9) \rightarrow OH(v'j') + Cl(^2P)$ [Zhang *et al.* J. Chem. Phys. **94**, 2704 (1991)]. The QM and experimental rotational distributions peak at similar OH(j') levels, but the QM distributions are significantly narrower than the measurements and previous quasi-classical dynamics studies. The OH(low j') populations observed in the measurements are nearly absent in the QM results. We have also performed quasi-classical trajectory with histogram binning (QCT-HB) calculations on these same benchmark surfaces. The QCT-HB rotational distributions, which are qualitatively consistent with measurements and classical dynamics studies using other surfaces, are much broader than the QM results. Application of a Gaussian binning correction (QCT-GB) dramatically narrows and shifts the QCT-HB rotational distributions to be in very good agreement with the QM results. The large QCT-GB correction stems from the special shape of the joint distribution of the classical rotational/vibrational action of OH products. We have also performed QM and QCT calculations for the transition, $O + HCl(v=0,T=300\ K) \rightarrow OH(v'j') + Cl$ from threshold to ~130 kcal mol^{-1} collision energy as a guide for possible future hyperthermal O-atom measurements. We find in general a mixed energy release into translation and rotation consistent with a late barrier to reaction. Angular distributions at high collision energy are forward peaked, consistent with a stripping mechanism. Direct collisional excitation channel cross sections, $O + HCl(v=0,T=300) \rightarrow O + HCl(v'=1)$, in the same energy range are large, comparable in magnitude to the reactive channel cross sections. Although the $^3A''$ state dominates most collision processes, above ~48 kcal mol^{-1}, the $^3A'$ state plays the major role in collisional excitation.

15. SUBJECT TERMS

16. SECURITY CLASSIFICATION OF:			17. LIMITATION OF ABSTRACT	18. NUMBER OF PAGES	19a. NAME OF RESPONSIBLE PERSON
					Dr. Marty J. Venner
a. REPORT	b. ABSTRACT	c. THIS PAGE	A	39	19b. TELEPHONE NUMBER *(include area code)*
Unclassified	**Unclassified**	**Unclassified**			(661) 275-5091

Preprint JULY 25, 2004

Quantum and Quasi-classical Studies of the $O(^3P) + HCl \rightarrow OH + Cl(^2P)$ Reaction Using Benchmark Potential Surfaces

Tiao Xie and Joel Bowman

Department of Chemistry and Cherry L. Emerson Center for Scientific Computation

Emory University

Atlanta, GA 30322

J. W. Duff and M. Braunstein*

Spectral Sciences, Inc.

Burlington, MA 01803

B. Ramachandran

Chemistry, College of Engineering & Science

Louisiana Tech University

Ruston, LA 71272

*Electronic mail address: matt@spectral.com

ABSTRACT

We have performed quantum mechanical (QM) dynamics calculations within the independent-state approximation with new benchmark triplet A" and A' surfaces [B. Ramachandran *et al.* J. Chem. Phys. **119**, 9590 (2003).] for the ro-vibronic state-to-state measurements of the reaction $O(^3P) + HCl(v=2,j=1,6,9) \rightarrow OH(v'j') + Cl(^2P)$ [Zhang *et al.* J. Chem. Phys. **94**, 2704 (1991)]. The QM and experimental rotational distributions peak at similar OH(j') levels, but the QM distributions are significantly narrower than the measurements and previous quasi-classical dynamics studies. The OH(low j') populations observed in the measurements are nearly absent in the QM results. We have also performed quasi-classical trajectory with histogram binning (QCT-HB) calculations on these same benchmark surfaces. The QCT-HB rotational distributions, which are qualitatively consistent with measurements and classical dynamics studies using other surfaces, are much broader than the QM results. Application of a Gaussian binning correction (QCT-GB) dramatically narrows and shifts the

QCT-HB rotational distributions to be in very good agreement with the QM results. The large QCT-GB correction stems from the special shape of the joint distribution of the classical rotational/vibrational action of OH products. We have also performed QM and QCT calculations for the transition, O + HCl(v=0,T=300 K) $\rightarrow$ OH(v'j') + Cl from threshold to ~130 kcal mol^{-1} collision energy as a guide for possible future hyperthermal O-atom measurements. We find in general a mixed energy release into translation and rotation consistent with a late barrier to reaction. Angular distributions at high collision energy are forward peaked, consistent with a stripping mechanism. Direct collisional excitation channel cross sections, O + HCl(v=0,T=300) $\rightarrow$ O + HCl(v'=1), in the same energy range are large, comparable in magnitude to the reactive channel cross sections. Although the ^{3}A'' state dominates most collision processes, above ~48 kcal mol^{-1}, the ^{3}A' state plays the major role in collisional excitation.

I. INTRODUCTION

The reaction, $O(^3P) + HCl(X^1\Sigma) \rightarrow OH(X^2\Pi) + Cl(^2P)$, is an important prototype for heavy-light-heavy (H-L-H) systems and hydrogen abstraction. The reaction is nearly thermo-neutral, with a ΔH of ~1.0 kcal mol^{-1} and a barrier of ~10.6 kcal mol^{-1} for the lowest adiabatic electronic state involved.[1] Experimental rate constant data are available from a number of initial vibrational levels of HCl over a broad temperature range.[2-8] Measurements of the relative populations for ro-vibronic transitions $O(^3P) + HCl(v=2,j=1,6,9) \rightarrow OH(v'j') + Cl(^2P)$ have been made in what was the first fully ro-vibronic state-to-state experiment.[9-10] With HCl(v=2) levels initially populated, relatively slow collisions of O + HCl occur above the reaction barrier, and OH(v'=0,1) with a large range of OH(j') levels are observed. Taken together, these measurements have shown many important insights including: a strong HCl(v) dependence of the rate constant, a vibrational-energy conserving tendency (vibrational adiabaticity), insensitivity of product rotational level to reagent rotational level, a fairly even partitioning of energy among translation, vibration, and rotation of products, and apparently two dynamical mechanisms that give rise to distinct rotational populations.

The wealth of experimental data and dynamical information make this reaction a test-bed for dynamics methods.[11-23] Using recent, highly accurate potential surfaces,[11-12] agreement between theory and measurements has been very good for the rate constant and the ro-vibronic state-to-state measurements in general.[13-14] However, important differences remain. Very recently, new benchmark surfaces[1] have been calculated and used with quantum mechanical dynamics (QM) to compute the thermal rate constant.[15] Although agreement is excellent up to 2,000 K, large differences between these calculations and measurements at higher temperatures point to a need for further investigations.

The main purpose of this paper is to report time-independent QM calculations with the new benchmark triplet surfaces of Ref. 1 for the ro-vibronic state-to-state measurements, $O(^3P) + HCl(v=2,j=1,6,9) \rightarrow OH(v'j') + Cl(^2P)$, of Ref. 10. The present calculations are a stringent test of the quality of the surfaces and will show the level of agreement that can be obtained between highly detailed measurements and nearly exact theory. It will also be the first time to our knowledge that these measurements have been modeled with quantum dynamics. A previous quasi-classical trajectory (QCT) study using the surface of Ref. 11 predicted the peak location

and spread of OH(j') rotational distributions and the OH(v=1)/OH(v=0) branching ratio generally very well.[11,13] For the surface Ref. 12, a previous QCT study showed that the spread of the OH(j') rotational distributions were reproduced well, but the OH(j') peak locations were too high in energy resulting in too hot a rotational distribution.[14] An important result from the present study is that the computed QM results have a significantly narrower distribution of rotational states than the measurements and previous QCT studies,[11,13,14] with the OH(low j') populations observed in the measurements being nearly absent in the QM results. Peak locations of the QM OH(j') populations are quite similar to the measurements, but the maxima of the relative rotational populations are much larger in general than the measurements and previous QCT studies. Possible implications of the present QM results are that the new benchmark surfaces are not adequate to describe the O + HCl(v=2,j) $\rightarrow$ OH(v'j') + Cl transitions and/or the measurements themselves require re-assessment. It could also be that the QM approach requires inclusion of spin-orbit coupling effects with nearby singlet states[24] or other kinds of electronic state coupling not taken into account in the present study.

We also performed quasi-classical trajectory calculations with the usual histogram binning (QCT-HB) on these same benchmark surfaces to evaluate how well this widely used method compares to exact QM methods for this fairly quantum system. The present QCT calculations on the benchmark surfaces are also a common denominator for comparisons with QCT-HB studies using other surfaces so that differences between surfaces can be assessed. A significant finding of the present study is that the QCT-HB rotational distributions are much broader than the QM results with the same benchmark surfaces. The QCT-HB results are similar to previous QCT-HB studies using other surfaces[11,13,14] and in fair agreement with measurements. The similarity of the QCT-HB results and previous classical studies implies that the new benchmark potential energy surfaces are perhaps dynamically similar to those used in previous studies,[11-14] although the barrier heights a different.

QCT and QM calculations for the same surfaces are also an opportunity to examine techniques that may correct classical methods. A simple proposed correction method is the Gaussian binning (QCT-GB) technique[25,26] that in spirit attempts to approximate a fully semi-classical approach. Instead of using all trajectories in a classical vibrational energy bin as in histogram binning (QCT-HB), the QCT-GB method heavily weights trajectories with energies

near the exact quantum vibrational level. This is intuitively appealing and automatically de-emphasizes trajectories not energetically allowed. It helps solve the common problem of rotational distributions that are too broad, extending too high in energy. In the present study the QCT-GB correction dramatically narrows and shifts the QCT-HB rotational distributions to an extent not before seen in other chemical systems, so that the QCT-GB and QM results are in very good agreement for all transitions. The striking consistency of the QM and QCT-GB results and their differences with measurements highlight the fact that detailed understanding of this chemical system is still far away.

As the effects of the QCT-GB correction are much larger and much different than in previous studies, we investigate the cause in a preliminary way by examining the classical rotational/vibrational action joint distribution of the OH products. Future work will investigate in detail the underlying fundamental reasons for the correction's apparent success in O + HCl and how the Gaussian-binning correction behaves in other systems. As many important chemical systems remain out of reach in the immediate future for an exact QM dynamics treatment, a reliable correction to a classical trajectory approach will be extremely useful.

We have also performed QM and QCT calculations for the transition, O + HCl(v=0,T=300 K) $\rightarrow$ OH(v',j') + Cl from threshold to ~130 kcal mol^{-1} collision energy. These calculations are intended to guide future hyperthermal O-atom measurements centered near 85.0 kcal mol^{-1} (8 km s^{-1}). Recently, hyperthermal O-atom beams have investigated novel chemistries for a number of systems.[27] The high translational energies in such a measurement would surmount the reaction barrier for O + HCl, without the need for internal excitation of the reagent HCl, and deposit large amounts of energy in products. We report on the excitation function, vibrational and rotational distributions of OH products, and the vibrationally resolved angular distributions. We note that above ~38.0 kcal mol^{-1}, the channel O + HCl(v=0,T=300) $\rightarrow$ OCl + H is energetically allowed. The present surfaces do not take the OCl + H channel into account, and they are not intended to be quantitative above ~40 kcal mol^{-1} even for the OH + Cl channel. At high energies therefore, the dynamical results presented here will only be qualitative. However, lacking other sources of data the present results at high energies will be an important starting point for hyperthermal measurement planning and for future theoretical studies in this energy regime. We find in general a mixed energy release into translation and rotation consistent with a late barrier to

reaction. Above ~35 kcal mol^{-1} the fraction of rotational energy in OH products exceeds vibration. The rotational distributions are extremely hot and should give rise to distinct OH band-head spectra. Angular distributions at high collision energy are forward peaked consistent with a stripping mechanism. We have also performed QCT calculations on the direct collisional excitation channel, O + HCl(v=0,T=300 K) $\rightarrow$ O + HCl(v'=1), with the same benchmark surfaces. Vibrational excitation cross sections are large, comparable in magnitude to the reactive channel cross sections.

The paper proceeds as follows. In section II we review the surfaces, and the QM and QCT dynamical methods used in this study. In section III, we present theoretical results for the $O(^3P)$ + HCl(v=0,T) $\rightarrow$ OH + Cl rate constant, the ro-vibronic state-specific transitions $O(^3P)$ + HCl(v=2,j=1,6,9) $\rightarrow$ OH(v'j') + $Cl(^2P)$, the transitions O + HCl(v=0,T=300 K) $\rightarrow$ OH(v'j') + Cl, and the transitions O + HCl(v=0,T=300 K) $\rightarrow$ O + HCl(v'=1), all with comparisons to measurements and other theoretical results where available. In section IV we summarize the results.

II. METHODS

A. Potential surfaces

The present study uses the two lowest triplet adiabatic surfaces for $O(^3P)$ + $HCl(X^1\Sigma)$, $^3A''$ and $^3A'$, as reported in Ref. 1 and generated from a computer program kindly provided by the authors of that study. The surfaces are fits of complete basis set extrapolated multi-reference configuration interaction calculations with a large basis set, and they are the most accurate surfaces available to date. The lower $^3A''$ state has a bent (136.0°) transition state geometry with a barrier of 10.60 kcal mol^{-1}, and the $^3A'$ transition state is linear with a barrier of 13.77 kcal mol^{-1} . Further details of the surfaces can be found in Ref. 1.

All scattering calculations were performed within the independent, non-interacting surface approximation. The repulsive $2^3A''$ state has not been included, and coupling to singlet surfaces is ignored. Dynamical results from the $^3A''$ and $^3A'$ surfaces are weighted by the following temperature dependent expression that attempts to account for the spin-orbit splitting of the overall triplet reagents:

$$f(T) = 3/(5 + 3e^{-228/T} + e^{-326/T}). \quad (1)$$

At 300 K, *f(T)* = 0.445, and at high temperature where all spin-orbit states become equally populated *f(T)* = 1/3. We note that use of Eq. (1) for inclusion of spin-orbit degeneracy is approximate as we are not accounting for fine-structure explicitly, and for low temperatures results in weights totaling greater than 1.0 if summed over all three electronic states.

B. Quantum dynamics

The QM calculations were done using the quantum reactive scattering code 'ABC'.[28] Detailed state-to-state reaction probabilities $P^J_{vjK,v'j'K'}(E)$ were calculated as a function of the total energy *E* and the total angular momentum *J*. From these probabilities the reaction cross sections summed over *J, K* and *K'* for a particular vj $\rightarrow$ v'j' transition were obtained from the standard expression,

$$\sigma_{vj,v'j'}(E) = \frac{\pi}{(2j+1)k_i^2} \sum_K \sum_J (2J+1) \sum_{K'} P^J_{vjK,v'j'K'}(E), \quad (2)$$

where k_i is the wave vector. The details of the scattering calculations for the O(^{3}P)+HCl reaction on the ^{3}A" and ^{3}A' surfaces are essentially the same as in a recent paper.[15]

For the O + HCl (v=2, j =1,6,9) $\rightarrow$ OH (v'=0,1,j') + Cl transition calculations, converged results were obtained with maximum values of *J* and *K*(*K'*) of 150 and 9, respectively. For the coupled channel aspect of the calculation we retained all reactant and product channels with internal energies less than E_{max} = 55.35 kcal mol^{-1} (relative to O + HCl (r_e)) and with diatomic rotational quantum numbers $j_{max} \leq 24$. A total of 2275 close-coupled equations were integrated using 120 hyperradii sectors between ρ_{min} = 1.8 a.u. for the ^3A" surface, 1.9 a.u. for the ^3A' surface and ρ_{max} = 16.0 a.u. for both surfaces. In order to simulate the experimentally measured[10] product OH relative v'j' populations, we calculated the relative populations following the approach given in previous QCT calculations.[11] Thus, the relative population *P(v',j')* is given by

$$P(v', j') = F(v', j') / F_{tot}, \quad (3)$$

where

$$F(v', j') = \sum_i f(E_{coll,i}) \sum_J (2J+1) \sum_{K,K'} P^J_{vjK,v'j'K'}(E_{coll,i}), \quad (4)$$

and

$$F_{tot} = \sum_{j'} [F(0, j') + F(1, j')]. \quad (5)$$

In Eq. (4) above, $f(E_{coll,i})$ is the fitted experimental initial translational energy distribution function described below, and $E_{coll} = E - E_{vj}$.

For the O + HCl(v=0,T=300 K) → OH(v',j') + Cl transition calculations, we applied the standard thermal averaging to the distribution of HCl internal states. Due to the low temperature of the system, the range of j and j' is smaller than for the O + HCl(v=2, j=1,6,9) calculations, and the cross sections were well converged with K_{max} equal to 6. However, since we are interested in higher collision energies, convergence with respect to J for E_{coll} = 33.2 kcal mol^{-1} (5 km s^{-1}) was not reached until J_{max} = 220. Higher collision energies require too much computational effort, so we stopped at E_{coll} =33.2 kcal mol^{-1}. All other parameters in the quantum reactive scattering calculations were the same as the calculations on the O + HCl (v=2, j =1,6,9) → OH (v'=0,1, j') + Cl transitions, except for the number of coupled channel equations which was reduced to 1729 as a result of the smaller K_{max}.

C. Classical dynamics

For the QCT calculations, we use standard Monte Carlo techniques.[29] Table I summarizes the convergence parameters used in the various QCT calculations, where b_{max} is the maximum impact parameter and Δt_{min} is the minimum integration time step for the variable time step integrator. The same procedure has been followed to model the experiments of Ref. 10 for the transitions the O + HCl(v=2, j =1,6,9) → OH(v'=0,1,j') + Cl. The relative populations P(v'j') were obtained analogous to the QM ones, and follow directly the approach described in previous QCT calculations.[11] The only difference from the QM calculations, is that instead of peforming the collision energy average, the relative OH(v'j') populations are obtained by directly sampling from the initial translational energy distribution described below for each trajectory.

Table I. Convergence parameters for QCT calculations.

	b_{max} (a.u.)	Δt_{min} (a.u.)	Number of Trajectories	Statistical Uncertainty
$O(^3P) + HCl \rightarrow OH + Cl$ rate constant	4.0 → 4.8 1000 K → 2500 K	0.01	5.e4 → 2.e4 1000 K→ 2500 K	<1 %
$O(^3P) + HCl(v=2,j=1,6,9) \rightarrow OH(v'j') + Cl(^2P)$	5.2	0.01	~8.e5 for each HCl(j)	<1% QCT-HB <10% QCT-GB
$O(^3P) + HCl(v=0,T=300) \rightarrow OH(v'j') + Cl(^2P)$	3.4-4.8	0.01	2.e5 $v \geq 6$ km s^{-1} 6.e4 $v \leq 5$ km s^{-1} per coll. energy	1%(v)-10%(j)
$O(^3P) + HCl(v=0,T=300) \rightarrow O(^3P) + HCl(v')$	3.4-4.8	0.01	2.e5 $v \geq 6$ km s^{-1} 6.e4 $v \leq 5$ km s^{-1} per coll. energy	1%(v)

To assign final internal energy states in the QCT calculations, we define the continuous rotational diatomic "quantum number", *j'*,

$$j' = J_r / \hbar - \tfrac{1}{2} \tag{6}$$

where J_r is the magnitude of the product diatomic angular momentum vector, $\boldsymbol{J_r}$. The continuous diatomic vibrational quantum number, *v'*, is assigned with the following standard semi-classical expression,

$$v' = \frac{1}{\pi\hbar}\int_{r_-}^{r_+}\left\{2\mu\left[\varepsilon_{\text{int}} - V_D(r) - \frac{J_r \cdot J_r}{2\mu r^2}\right]\right\}^{1/2} dr - \frac{1}{2}, \tag{7}$$

where $r_\pm$ are the classical turning points, ε_{int} is the internal energy, $V_D(r)$ is the diatomic potential, and μ is the reduced mass. For the QCT-HB calculations, *v'* and *j'* for a given trajectory are assigned to the nearest integer bin with equal weighting wherever they fall within the bin. When these "quantum numbers" are translated back into integer bins, they can correspond to energetically closed channels, a well-known problem of QCT-HB. As pointed out in Refs. 25 and 26, one can lessen this problem by applying a Gaussian shaped weighting function to the classical trajectories (QCT-GB) such that the trajectories with vibrational quantum numbers closest to an integer value are most heavily weighted, and those near the edges

of a bin are effectively not considered. The weighting function used in the present work has the form,

$$G(v) = \frac{\beta}{\sqrt{\pi}} \exp(-(\beta(v'-n))^2), \quad (8)$$

where n is the bin integer value $n = (0,1,2, ...)$ and β is the bin-width parameter. For the QCT-GB results, we used a value of β=16.651 which corresponds to a full-width-half-maximum (FWHM) of 0.1. This width is quite narrow and effectively removes a large fraction of the trajectories. The results were insensitive to the exact value of β, varying by 2-4 % over a value corresponding to FWHM from 0.05 to 0.2. The QCT-GB correction has been used in a number of recent studies, and the major effect has been to remove the hotter, energetically closed rotational populations. We note that in spirit the correction attempts to achieve a semi-classical approach. However, since only a fraction of the trajectories falling in a bin contribute significantly, many more trajectories need to be computed for statistical accuracy comparable to QCT-HB. As an indication of the comparative statistics between QCT-HB and QCT-GB, Table II gives the number of trajectories for all reactive transitions, O + HCl(v=2,j=1,6,9) → OH(v'=1,j') + Cl, for the QCT-HB and QCT-GB trajectory calculations. Of the 800,000 classical trajectories run for these transitions, 61614 contributed to OH product. Of these 41371 contributed to the QCT-HB result for v'=1 ($0.5 \le v' \le 1.5$), with 6163 in the range $0.95 \le v' \le 1.05$ most important for QCT-GB with a full-width half-maximum of 0.1

Table II. Number of QCT reactive trajectories for the transition O + HCl(v=2,j=1,6,9) → OH(v'=1,j') as a function of the bin width.

j	$0.5 \le v' \le 1.5$	$0.9 \le v' \le 1.1$	$0.95 \le v' \le 1.05$
1	41371	12527	6163
6	10982	2488	1301
9	6898	2349	1145

D. Initial translational energy distributions for O + HCl(v=2,j=1,6,9) → OH(v',j') + Cl

Modeling of the state specific ro-vibronic experiments of Ref. 10 for the ro-vibronic measurements of the transitions, O + HCl(v=2,j=1,6,9) → OH(v',j') + Cl, is complicated by the fact that collisions take place over a range of initial translational energies. Ultimately, the center

of mass frame translational energy distribution of the O + HCl reagents must account for the relative thermal motion of the HCl with respect to the initial O atom velocities imparted from photodissociation of NO_2.[30-33] The general form of the translational energy distribution for such collisions has been derived in the literature.[31] For O + HCl Ref. 14 reports, without supporting details, a reagent translational energy distribution that is Boltzmann-like centered at ~2.3 kcal mol^{-1} and extending to ~8.1 kcal mol^{-1}. Since there remains some ambiguity about the actual initial translational energy distribution for O + HCl, in Appendix A we explicitly give the functional form for the translational energy distribution specifically applied to the O + HCl measurements of Ref. 10, and the details of its derivation are discussed. We present a Monte Carlo sampling method to determine initial collision velocities based on this functional form that is particularly convenient and efficient for the present QCT calculations. The initial translational energy distributions obtained are similar to those reported in Ref. 14.

III. RESULTS

A. Rate constant for O + HCl(v=0) → OH + Cl

Figure 1 shows the present calculated QCT-HB and QM results[15] along with recent experimental results between 1,000 K and ~3,000 K. Both QCT-HB and QM results include the $^3A''$ and $^3A'$ surfaces. As shown previously, the QM results are in excellent agreement with measurements up to ~2,000 K. Above this temperature, it was shown that the OCl channel is likely not contributing, and the differences between theory and measurement remain an open issue. The QCT-HB results are about a factor of two lower than the QM results at 1,000 K, but by 2,500 K they are nearly identical. This is consistent with a previous study using other surfaces at lower temperatures[14] and with the expectation that tunneling is becoming less important with increasing energy. These calculations help confirm that the O+HCl potentials are being used consistently in the quantum and classical scattering calculations.

B. Cross sections and relative populations for O + HCl(v=2,j=1,6,9) → OH(v'j') + Cl

We wish to model the measurements of Ref. 10 for the transitions, O + HCl(v=2,j=1,6,9) → OH(v'j') + Cl. As discussed earlier, the initial collision energies have a Boltzmann-like spread from 0 up to ~8 kcal mol^{-1}. To understand the impact of this energy distribution and for a more

straightforward comparison between QM and QCT results, in Figure 2 we show the energy dependence of the cross sections for the present calculated QCT-HB and QM results for the transitions O + HCl(v=2,j=1,6,9) → OH(v'=0,1) + Cl. For comparison purposes these results use only the ^{3}A'' surface. (The ^{3}A' surface makes a relatively small contribution to the cross section.) Except very near threshold, the agreement between QCT-HB and QM results is remarkably good including the local structure between 0.1 and 0.2 eV where QCT calculations were done for HCl(v=2,j=6,9). (We wish to emphasize that the QCT cross sections at fixed energy presented in Figure 2 were not used to generate results for comparison purposes with the measurements of Ref. 10. To compute relative populations, QCT results were obtained by directly sampling from the initial translational energy distribution discussed earlier.) We note that as in Ref. 14 Fig. 11, the HCl(v=2,j=1) cross section is much larger than the other transitions. However, all cross sections presented here are about a factor of 2 larger than those in Ref. 14. The relative magnitude ordering of the HCl(v=2,j) cross sections of the present results are much different than those using the surface of Ref. 11.

We note that the collision energy distribution in the measurements of Ref. 10 are Boltzmann-like with a maximum near 0.1 eV, but the calculated energy dependent cross sections continue to rise rapidly after this energy. The net effect is that collisions near 0.2 eV appear to be the most important. Furthermore, we have found that results for a fixed collision energy around 0.2 eV are quite similar to results taking into account the full initial translational energy distribution.

Figure 3 shows the present theoretical results, QM, QCT-HB (histogram binning), and QCT-GB (Gaussian binning), along with the measurements of Ref. 10 for the transitions O + HCl(v=2,j=1,6,9) → OH(v'=0,1,j') + Cl in terms of relative populations for each initial HCl(v=2,j) state. The theoretical results use the full initial translational energy distribution discussed earlier and both ^{3}A'' and ^{3}A' states.

A significant result of the present calculations as shown in Figure 3 is that the QM relative populations are much narrower and larger at the peak than the measurements, with the prominent OH(low j') populations in the measured results nearly absent in the QM results. The peak locations of the rotational populations agree very well between the QM and experimental results, especially for OH(v'=1). The differences between QM and experimental results are consistent across the HCl(v=2,j) initial states and extend far beyond measured error bars. This may mean

that the new benchmark surfaces are not adequate to describe the O + HCl(v=2,j) → OH(v'j') + Cl transitions and/or the measurements themselves require re-assessment. It may also point to the importance of spin-orbit coupling effects with nearby singlet states[24] or other kinds of electronic state interactions not taken into account in the present study. We note for example that Ref. 10 measures the OH $^2\Pi_{3/2}$ component only, and this may have to be explicitly accounted for in the modeling.

As a point of reference, the present QCT-HB results are in fair agreement with the measurements, although consistently extending too high in OH(j') and predicting an OH(j') maximum that is too low in OH(j'). The QCT-HB results have the same level of agreement with earlier QCT results using a different surface.[11,13] The largest difference between the present QCT-HB results and measurements occur for HCl(v=2,j=6).

Another significant finding of the present study is that the QCT-GB results are dramatically different from the QCT-HB results and closely resemble the QM results for all transitions. The QCT-GB correction, in addition to lessening the very high j' populations as seen in earlier studies on other systems,[25] severely diminishes the low j' populations, narrowing and shifting the j' distribution to match the QM results very well. Since the QCT-GB correction seen here is far larger and different than seen in other systems, we have examined the classical joint vibrational/rotational (continuous) distributions to understand the underlying mechanism for its apparent success. In Figure 4 we show a contour plot of the joint probability as a function of the continuous classical vibrational and rotational quantum numbers using trajectories for the transition O + HCl(v=2,j=1) → OH(v'j') + Cl. The contours have a distinct ridge-like shape along a line of high-j_{cl}, low-v_{cl} and extend to low-j_{cl}, high-v_{cl}, cutting off on the high energy side at the maximum available product energy. The ridge extends from the maximum near v_{cl}=1.25, j_{cl}=7.5 toward the low-v_{cl},high-j_{cl} corner, and appreciably stretches into the v_{cl}=2 bin.

For O + HCl(v=2,j=1) → OH(v'=0,j') + Cl transitions for example, QCT-HB will use all trajectories with v_{cl} between –0.5 and 0.5 with equal weighting, while QCT-GB will weight the trajectories with a Gaussian function such that those trajectories within the shaded band around v_{cl} =0.0 will be very heavily weighted. Because of the ridge-like shape of the probability and its orientation, it is clear how application of the Gaussian weighting narrows the rotational distribution. Because within a full bin the probability is weighted toward high v_{cl} and low-j_{cl},

application of the weighting function removes a great deal of high-v(low-j) populations. It is also interesting that weighting recovers the QM relative population magnitudes. Although promising, this work is preliminary, and we do not report a Gaussian binning correction to other results in this paper. But we do note that the Gaussian binning apparently has only a small affect on vibrational and total cross sections. Future work will investigate in detail the underlying fundamental reasons for the correction's apparent success in O + HCl and how the Gaussian-binning correction behaves in O+HCl transitions and in other systems.

Table III gives total and fractional product energies as a function of initial HCl(j) level. The experiment entries are taken from Ref. 10. We adopt their convention for defining energies for a more direct comparison: $\langle E_{tot'} \rangle$ is defined as the sum of initial vibrational energy, average initial translational energy, initial rotational energy and the heat of formation, $\langle E_{v'} \rangle$ is the average final OH vibrational energy with respect to the OH zero point, $\langle E_{r'} \rangle$ is the average final OH rotational energy, and the average final translational energy is defined $\langle E_{T'} \rangle = \langle E_{tot'} \rangle - (\langle E_{v'} \rangle + \langle E_{r'} \rangle)$. We also adopt the convention for the average fractional final energies, $\langle f'_{v',r',T'} \rangle = \langle E_{v'},E_{r'},E_{T'} \rangle / \langle E_{tot'} \rangle$. The table entries reflect results evident from the figures. Since the low OH(j') populations observed in the measurements are nearly absent in the QM and QCT-GB results, the average rotational energy fraction in the QM and QCT-GB results are larger than the measurements for all transitions. In fact, for all transitions the QM fractional rotational energies are larger than the QM fractional vibrational energies, which is opposite to what is observed experimentally. The fractional amount of internal energy is greater for all theoretical results compared to measurements, and the partitioning of energy between vibration and rotation in the theoretical results varies more as a function initial HCl(j) level than the measurements. The QCT-HB average rotational fractions are in fair agreement with the experimental results. Including contributions from the OH(v'=2) QCT results makes the fraction of energy going into vibration much larger, as expected from examination of the joint classical vibration/rotation actions.

Table III. Average total and fractional energy partitioning for OH(v'j') product for transitions HCl(v=2,j) → OH(v'j') + Cl. Main entries include OH(v'=0,1) states and for QCT results are obtained by assigning energies after quantum binning. QCT entries in parentheses include all transitions to v'=0,1, and 2 OH states, and they were obtained by assigning energies of classical trajectories directly, before binning into quantum OH(v'j') final states. All energies are in kcal mol^{-1}.

		Experiment Ref. 10	QM	QCT-HB	QCT-GB
	$<E_{tot'}>$	18.6			
	$<E_{v'}>$	7.3	8.2	8.3	8.2
	$<E_{r'}>$	5.9	7.3	6.2	7.4
HCl(j=1)	$<E_{T'}>$	5.4	3.1	4.0	3.1
	$<f_{v'}>$	0.395	0.439	0.449(0.547)	0.441(0.440)
	$<f_{j'}>$	0.320	0.495	0.331(0.272)	0.395(0.361)
	$<f_{T'}>$	0.285	0.166	0.220(0.181)	0.164(0.199)
	$<E_{tot'}>$	19.8			
	$<E_{v'}>$	7.6	8.0	9.2	9.2
	$<E_{r'}>$	6.4	8.5	5.4	7.2
HCl(j=6)	$<E_{T'}>$	5.8	3.3	5.2	3.5
	$<f_{v'}>$	0.386	0.403	0.464(0.622)	0.463(0.504)
	$<f_{j'}>$	0.325	0.431	0.273(0.210)	0.363(0.310)
	$<f_{T'}>$	0.289	0.166	0.263(0.168)	0.174(0.186)
	$<E_{tot'}>$	21.2			
	$<E_{v'}>$	8.2	8.5	8.9	8.7
	$<E_{r'}>$	7.0	8.6	7.0	8.8
HCl(j=9)	$<E_{T'}>$	6.0	4.1	5.3	3.8
	$<f_{v'}>$	0.386	0.402	0.421(0.611)	0.408(0.602)
	$<f_{j'}>$	0.331	0.406	0.330(0.212)	0.414(0.242)
	$<f_{T'}>$	0.284	0.192	0.249(0.177)	0.178(0.156)

Table IV gives the cross section summed over OH(v'=0,1,j') as a function of HCl(j) level. Although the QCT and QM results are different in magnitude, they show a very similar decrease

in cross section as a function of the initial HCl(j): a factor of 3.4 for QCT-HB and 5.3 for QM in going from HCl(j=1) to HCl(j=9). In contrast, the experimental results *increase* as a function of HCl(j) by a factor of 1.5 ±0.5 in going from HCl(j=1) to HCl(j=9).[10]

Table IV. Total cross section summed over all final states OH(v'j') as a function of HCl(j) level for the transition HCl(v=2,j) → OH(v',j') + Cl.

j	QCT-HB σ(a.u.)	QM σ(a.u.)
1	1.294	2.869
6	0.440	0.685
9	0.386	0.546

The vibrational branching ratios, σ(v'=1)/σ(v'=0) are shown in Table V as a function of HCl(j) level. For HCl(j=1) all theoretical results are in fair agreement with each other and they are larger than the experimental results. The QM and experimental results are in fair agreement for HCl(j=6,9). However, the QCT results are all consistently much larger than the experiment, especially for HCl(j=6), although the QCT-GB correction does improve agreement with the QM results. The under-estimate of the v'=0 level contribution in the QCT-HB results is not fully recovered in the QCT-GB correction.

Table V. Vibrational Branching Ratios OH(v'=1)/OH(v'=0) for O + HCl(v=2,j) → OH(v',j') + Cl

	j=1	j=6	j=9
Experiment	2.6±0.1	3.0±0.1	4.1±0.2
QM	4.0	3.6	5.1
QCT-HB	4.5	9.1	7.0
QCT-GB	4.1	8.7	5.6

C. Cross sections for O + HCl(v=0,T=300 K) → OH(v'j') + Cl

As a guide to possible future hyperthermal O-atom beam measurements centered near ~8 km s^{-1} (85.0 kcal mol^{-1}), which surmount the reaction energy barrier through reagent translation as opposed to internal energy, we present results for the transition O + HCl(v=0,T=300 K) → OH(v'j') + Cl from threshold to 10 km s^{-1} collision velocity (~133 kcal mol^{-1}). This is the first time to our knowledge that results for this system have been presented above ~20 kcal mol^{-1}. The upper energy range of these calculations is far beyond the energy threshold for the OCl + H channel at (~38 kcal mol^{-1}) and the reported valid range of the potential surfaces even for the OH + Cl channel. The present results above ~40 kcal mol^{-1} (~5.5 km s^{-1}) use what is really an extrapolation of the fitted surfaces, and so there is a large uncertainty associated with any dynamical results generated from them. However, the present calculations yield important qualitative information and serve as a baseline for future work.

Figure 5 shows results for the QM and QCT-HB reactive cross section for O + HCl(v=0,T=300 K) → OH(v') + Cl as a function of relative collision velocity. The QM results include only the ^{3}A'' surface and the QCT-HB results include both surfaces. Figure 5a shows the QCT-HB total reactive cross section, the ^{3}A'' and ^{3}A' component contributions, and the QM results for the ^{3}A'' surface alone. There is excellent agreement between the QM and QCT-HB results. They show a steep rise from threshold and a leveling off of the total cross section which is dominated by the ^{3}A'' contribution. Above ~4 km s^{-1} (21.3 kcal mol^{-1}) the cross section remains constant over a large velocity range. Figure 5b shows the vibrationally resolved cross sections as a function of velocity. There is generally good agreement between QM and QCT-HB results, but the v'=0 cross sections are underestimated and the v'=1 are over-estimated by the QCT-HB method, consistent with our findings in Table V. There is a large falloff in the cross section with vibrational quanta, especially near threshold, with most of the product energy going into translation and rotation. This is consistent with a late barrier picture of the energy release.

Figure 6 shows the OH(j') cross sections for OH(v'=0,1) at collision velocities of 4, 6, and 8 km s^{-1} (21.3, 47.8, and 85.0 kcal mol^{-1}, respectively). QCT-HB results are shown for all velocities, and QM results are shown at 4 km s^{-1}. The rotational distributions peak approximately between j'=10 and j'=20 (~6 and ~23 kcal mol^{-1}) and extend up to j'=35 (68 kcal mol^{-1}) at 8 km s^{-1}. At 4 km s^{-1}, agreement between QM and QCT-HB results is very good with the QM results

slightly narrower, but with the same peak locations. The QCT-HB results extend farther in OH(j') than the QM results, behavior that could perhaps be corrected with Gaussian binning. Unlike the previous O + HCl(v=2,j) QM and QCT-GB results, however, low OH(j') populations are significant, and it would be interesting to see if the QCT-GB correction can be effectively applied here. Figure 7 shows the average rotational quantum number of the OH(j') product as a function of collision velocity. There is good agreement between the QCT-HB and QM results except near threshold, showing the steep increase in OH(j') with velocity. Figure 8 shows the fractional energy release in products as a function of collision velocity. Above 5 km s^{-1}, the fraction of energy in rotation exceeds vibration. The high OH(j') populations will produce a distinct band-head OH spectrum for the nascent products, something that should be experimentally observable. The strong translational and rotational energy release in this reaction is consistent with the late barrier in the ^{3}A'' potential energy surface. Finally, Figure 9 shows the OH(v') angular distribution as a function of the center of mass scattering angle. The dominant v'=0 and v'=1 cross sections are quite forward peaked indicating a stripping mechanism.

D. Collisional excitation of HCl: O + HCl(v=0,T=300 K) $\rightarrow$ O + HCl(v'=1)

Hyperthermal O atom observations may also contain a substantial collisional excitation component. To investigate this possibility we have performed QCT-HB calculations on the transition O + HCl(v=0,T=300 K) $\rightarrow$ O + HCl(v'=1). The results are shown in Figure 10 broken down into ^{3}A'' and ^{3}A' components. Near threshold, the ^{3}A'' surface contribution dominates and the cross sections are relatively small. Above 6 km s^{-1}, however, the ^{3}A' surface contribution becomes most important in what is likely a different excitation mechanism. It could be that trajectories that are reactive on the ^{3}A'' surface create vibrational excitation very effectively on the ^{3}A' surface. At these high velocities, the total cross section begins a steep rise making collisional excitation channel comparable in magnitude to the reactive channel.

IV. SUMMARY

We have performed time-independent quantum mechanical (QM) dynamics calculations with the new benchmark triplet surfaces of Ref 1 for the ro-vibronic state-to-state scattering, O(^{3}P) + HCl(v=2,j=1,6,9) $\rightarrow$ OH(v'j') + Cl(^{2}P), of Ref. 10 and compared to experiment. Although the

OH(j') peak locations agree well between QM results and experiment, the QM results have a significantly narrower distribution of rotational states than measurements and previous classical dynamics studies. The OH(low j') populations observed in the measurements are nearly absent in the QM results. Possible implications of the present QM results are that the new benchmark surfaces are not adequate to describe the O + HCl(v=2,j) → OH(v'j') + Cl transitions and/or the measurements themselves require re-assessment. It could also be that the QM approach requires inclusion of spin-orbit coupling effects with nearby singlet states or other kinds of electronic state interactions not taken into account in the present study.

We have also performed quasi-classical trajectory with histogram binning (QCT-HB) calculations on these same benchmark surfaces. The QCT-HB rotational distributions, which are qualitatively consistent with measurements and classical dynamics studies using other surfaces, are much broader than the QM results. Application of a Gaussian binning correction (QCT-GB) dramatically narrows and shifts the QCT-HB rotational distributions to be in very good agreement with the QM results. The cause of the large QCT-GB correction stems from the special shape of the classical rotational/vibrational action joint distribution of OH products. Future work will investigate in detail the underlying fundamental reasons for the correction's apparent success in O + HCl and how the Gaussian-binning correction behaves in other systems. The striking consistency of the QM and QCT-GB results and their differences with measurements highlight the fact that detailed understanding of this chemical system is still far away.

We have also performed QM and QCT calculations for the reactive transitions, O + HCl(v=0,T=300 K) → OH(v',j') + Cl from threshold to ~130 kcal mol^{-1} collision energy as a guide for possible future hyperthermal O-atom measurements. Above ~40 kcal mol^{-1} we expect only qualitative results as this is beyond the reported valid range of the surfaces. However, these results will be an important baseline for future measurements and theoretical studies. We find in general a mixed energy release into translation and rotation consistent with a late barrier to reaction. The rotational distributions are extremely hot and should give rise to distinct OH band-head spectra. Angular distributions at high collision energy are forward peaked consistent with a stripping mechanism. We have also performed QCT calculations on the direct collisional excitation channel, O + HCl(v=0,T=300 K) → O + HCl(v'=1), in the same energy range with the

same benchmark surfaces. Vibrational excitation cross sections are large, comparable in magnitude to the reactive channel cross sections. Although the $^3A''$ state dominates most collision processes, above ~48 kcal mol^{-1}, the $^3A'$ state plays the major role in collisional excitation.

ACKNOWLEDGEMENTS

M. B. and J. W. D. acknowledge support through a Small Business Innovative Research (SBIR) award from the Missile Defense Agency (MDA) Contract No. F04611-03-C-0015. M. B. and J. W. D. thank Dr. M. Venner of the Air Force Research Laboratory for technical oversight of this work. M.B. and J. W. D. also acknowledge support from the DoD through contract F19628-00-C-0006. JMB thanks the National Science Foundation (CHE-0131482) for support.

APPENDIX A. O+HCl translational energy distribution for the measurements of Ref. 10.

In this appendix, we review the derivation of the center of mass frame reagent translational energy distribution for the ro-vibronic state-specific measurements of Ref. 10, O + HCl(v=2,j=1,6,9) $\rightarrow$ OH(v′,j′) + Cl. The reagent O-atoms are initially formed from photodissociation of NO_2. The resulting measured O atom velocity distribution of Ref. 32 (represented by the sum of the two Gaussians) is shown in Figure A1. The O atom velocity in this figure is in the center of mass frame of the NO_2 precursor. The lower velocity Gaussian-shaped peak corresponds to formation of NO(v=1) and the higher velocity peak to formation of NO(v=0). The explicit form used to model this distribution is,

$$f(u) = A\exp(-(a(u-u_1))^2) + B\exp(-(b(u-u_2))^2), \qquad \text{(A1)}$$

where u_1 = 890 m s^{-1}, u_2 = 1400 m s^{-1}, a = 4.6353e-3 s m^{-1}, b = 4.6353e-3 s m^{-1}, A = 0.847, and B = 0.997.

To model the O + HCl measurements of Ref. 10, we need the O + HCl center of mass frame relative velocity distribution. First, the velocity in the NO_2 frame is averaged over the thermal distribution of the NO_2 precursor, which results in an O atom distribution in the laboratory frame (Eq. 1 of Ref. 30) for a given speed, say v. Then v is averaged over the HCl

thermal distribution, as originally done in Ref. 33 (see, also Eq. 2 of Ref. 30). The resultant conditional relative velocity distribution is then averaged over the O atom distribution in the laboratory frame as described by Eq. 1 of Ref. 30, resulting in a relative velocity (speed) distribution in the O + HCl frame for a single value of u (Eq. 3 of Ref. 30). If the photodissociation process resulted in a single velocity value, we would simply use Eq. 3 Ref. 30. However, since we have a distribution of velocities given by Ref. 32., Eq. 3 of Ref. 30 is then averaged over the measured O atom distribution shown above. The resulting expression is given by Eq. (8) of Ref. 31, which reduces to Eq. 3 of Ref. 30 if the experimental distribution from the photodissociation process is given by $\delta(v\text{-}v_{exc})$.

Explicitly, for the processes, AB + hv $\rightarrow$ A + B and A + C $\rightarrow$ products, the final expression for the A + C velocity distribution in the center of mass frame used in the present QCT calculations is:

$$f(v_{coll}) = \left(\frac{\gamma}{\pi}\right)^{1/2} \int_0^\infty du f(u) u^2 \left[\frac{v_{coll}}{u}\right] \left\{\exp(-\gamma(u - v_{coll})^2 - \exp(-\gamma(u + v_{coll})^2\right\}. \quad \text{(A2)}$$

Here $\gamma = \frac{m_c m_{ab}}{m_a + m_b + m_c}$, u is the velocity (measured) in the AB center of mass frame, *f(u)* is the velocity distribution given in Eq. A1, and v_{coll} is the velocity in the A + C center of mass frame. In the present modeling, NO_2 + hv $\rightarrow$ O + NO and O + HCl $\rightarrow$ OH + Cl, so that A = O, B=NO, and C = HCl. Eq. A2 is particularly convenient for selecting initial O + HCl velocities for QCT calculations. In the present QCT calculations we select the initial O + HCl velocities in two steps:

1) Select u from $duf(u)u^2$.

2) Given u, select v_{coll} from $\left[\frac{v_{coll}}{u}\right]\left\{\exp(-\gamma(u - v_{coll})^2 - \exp(-\gamma(u + v_{coll})^2\right\}$.

The resulting O+HCl relative speed distribution from Eq. A2 is shown in Figure A2 as the $f_{O\text{-}HCl}(v)$ curve (solid line). Also shown is the kernel distribution, Eq. A1, times the velocity squared as a reference (dashed line). Figure A3 shows the relative translational energy distribution for O+HCl center of mass collisions. To judge the reasonableness of the distributions, consider the approximate FWHM for a (single) relative collision energy of ~0.1

eV. Eq. (4) of Ref. 30 estimates the FWHM to be 0.094 eV. The two maxima in the measured O-atom distribution of Ref. 32 are separated by ~0.067 eV. It is not surprising that the thermal averaging washes out the structure in the measured O atom distribution.

REFERENCES

1. B. Ramachandran and K. A. Peterson, J. Chem. Phys. **119**, 9590 (2003).

2. C. C. Hsiao, Y. P. Lee, N. S. Wang, and M. C. Lin, J. Phys. Chem. **106**, 10231 (2002).

3. K. Mahamud, J.-S. Kim, and A. Fontjin, J. Phys. Chem. **94**, 2994 (1990).

4. R. D. H. Brown, and I. W. N. Smith, Int. J. Chem. Kin. **7**, 301 (1975).

5. D. Arnoldi and J. Wolfrum, Chem. Phys. Lett. **24**, 234 (1974).

6. R. D. H. Brown, G. P. Glass, and I. W. M. Smith, Chem. Phys. Lett. **32**, 517 (1975).

7. R. G. Mcdonald and C. B. Moore, J. Chem. Phys. **68**, 513 (1978).

8. J. E. Butler, J. W. Hudgens, M. C. Lin, and G. K. Smith, Chem. Phys. Lett. **58**, 216 (1978).

9. D. J. Rakestraw, K. G. McKendrick, and R. N. Zare, J. Chem. Phys. **87**, 7341 (1987).

10. R. Zhang, W. J. van der Zande, M. J. Bronikowski, and R. N. Zare, J. Chem. Phys. **94**, 2704 (1991).

11. R. Ramachandran, E. A. Schrader, S. J. Sanekowitsch, and R. E. Wyatt, J. Chem. Phys. **111**, 3862 (1999).

12. H. Koizumi, G. C. Schatz, M. S. Gordon, J. Chem. Phys. **95**, 6421 (1991).

13. B. Ramachandran, J. Chem. Phys. **112**, 3680 (2000).

14. F. J. Aoiz, L. Benares, J. F. Castillo, M. Menendez, and J. E. Verdasco, Phys. Chem. Chem. Phys. **1**,1149 (1999).

15. T. Xie, J. M. Bowman, K. A. Peterson, and B. Ramachandran, J. Chem. Phys. **119**, 9601 (2003).

16. S. Skokov, S. Zou, J. M. Bowman, T. C. Allison, D. G. Truhlar, Y. Lin, B. Ramachandran, B. C. Garrett, and B. J. Lynch, J. Phys. Chem. A **105**, 2298 (2001).

17. K. Nobusada and H. Nakamura, J. Phys. Chem. A **103**, 6715 (1999).

18. W. H. Thompson, and W. H. Miller, J. Chem. Phys. **106**, 142 (1997); **107**, 2164E.

19. B. Poirier, J. Chem. Phys. **108**, 5216 (1998).

20. F. Matzkis, and U. Manthe, J. Chem. Phys. **112**, 130 (2000).

21. L. Wang, C. Kalyanaraman, A. B. McCoy, J. Chem. Phys. **110**, 11221 (1999).

22. 22. S. Skokov, T. Tsuchida, S. Nanbu, J. M. Bowman, and S. K .Gray, J. Chem. Phys. **113**, 227 (2000).

23. A. Persky and M. Broida, J. Chem. Phys. **81**, 4352 (1984).

24. M. Kneba and J. Wolfrum, Ann. Rev. Phys. Chem. **31**, 47 (1980).

25. L. Banares, F. J. Aoiz, P. Honvault, B. Bussery-Honvault, and J.-M. Launey, J. Chem. Phys. **118**, 565 (2003).

26. L. Bonnet and J. C. Rayez, Chem. Phys. Lett. **277**, 183 (1997).

27. D. J. Garton, T. K. Minton, D. Troya, R. Pascual, and G. C. Schatz, J. Phys. Chem. A **107**, 4583 (2003).

28. D. Skouteris, J. F. Castillo, and D. E. Manolopoulos, Comput. Phys. Commun. **133**, 128 (2000).

29. D. G. Truhlar and J. T. Muckerman, "Reactive Scattering Cross Sections III: Quasiclassical and Semiclassical Methods", in *Atom Molecule Collision Theory*, R. B. Bernstein editor, Plenum, New York, 1979.

30. W. J. van der Zande, R. Zhang, R. N. Zare, K. G. McKendrick, and J. J. Valentini, J. Phys. Chem. **95**, 8205 (1991).

31. M. Brouard, S. P. Dixon, P. A. Enriquez, and J. P. Simons, J. Chem. Phys. **97**, 7414 (1992).

32. V. P. Hradril, T. Suzuki, S. A. Hewitt, P. L. Houston, B. J. Whitaker, J. Chem. Phys. **99**, 4455 (1993).

33. P. J. Chantry, J. Chem. Phys. **55**, 2746 (1971).

Figure Captions:

Figure 1. Thermal rate constant for O + HCl(v=0) → OH + Cl from 1,000-3,000 K. ▫, measurements of Ref 3; ×, measurements of Ref. 2; -----, QM results of Ref. 15, —•—, present QCT-HB results.

Figure 2a-c. Vibrationally resolved cross sections as a function of energy for the transitions O + HCl(v=2,j=1,6,9) → OH(v'=0,1) + Cl. ▫, QM results for v'=0; ▩, QM results for v'=1; ◇, QCT-HB results for v'=0; ◆, QCT-HB results for v'=1.

Figure 3a-c. Relative populations of OH(v'j) as a function of OH(j') level for the transitions O + HCl(v=2,j=1,6,9) → OH(v'=0,1) + Cl. ○, Experimental results of Ref. 10 for v'=0; •, Experimental results of Ref. XXX for v'=1; ▫, QM results for v'=0; ▩, QM results for v'=1; ◇, QCT-HB results for v'=0; ◆, QCT-HB results for v'=1; ▵, QCT-GB results for v'=0; ▲, QCT-GB results for v'=1.

Figure 4. Joint probabilities of the continuous QCT rotational (j_{cl}) and vibrational (v_{cl}) action for the transition O + HCl(v=2,j=1) → OH(v'j') + Cl. The contours (0.9, 0.7, 0.5, 0.3, 0.1, and 0.05) are normalized such that the maximum is 1.0 (indicated by an *). Results include contributions from both the ^{3}A'' and ^{3}A'electronic states.

Figure 5. Total and vibrationally resolved cross sections for O + HCl(v=0,T=300) → OH + Cl as a function of relative collision velocity. (a) Total cross sections for O + HCl(v=0,T=300) → OH + Cl and their electronic components. ◆, QCT-HB total cross section including the ^{3}A'' and ^{3}A' states, ▫, QM results for the ^{3}A'' state up to 5 km s^{-1}; ◇, QCT-HB results for the ^{3}A'' state; ⬙, QCT-HB results for the ^{3}A' state;. (b) Total vibrationally resolved cross sections for O + HCl(v=0,T=300) → OH(v') + Cl and their electronic components. ◆, QCT-HB total cross including ^{3}A'' and ^{3}A' states for v'=0,1,, and 2; ◇, QCT-HB total cross section only including the ^{3}A'' state for v'=0,1, and 2; ▫, QM total cross section for the ^{3}A'' state only up to 5 km s^{-1} for v'=0,1, and 2.

6a-c. Rotationally resolved cross sections versus OH(j') for the transitions O + HCl(v=0,T=300) → OH(v'=0,1,j') + Cl at 4, 6 and 8 km s^{-1}, respectively. ▫, QM results at 4 km s^{-1} for v'=0; ▓, QM results at 4 km s^{-1} for v'=1; ◇, QCT-HB results at 4, 6, and 8 km s^{-1} for v'=0; ◆, QCT-HB results at 4, 6, and 8 km s^{-1} for v'=1.

7. Average OH(j') quantum number versus relative collision velocity for the transitions O + HCl(v=0,T=300) → OH(v'j') + Cl summed over v'. ▓, QM results; ◆, QCT-HB results.

8. Fractional energy disposal into OH products for the QCT-HB results versus relative collision velocity for the transition O + HCl(v=0,T=300) → OH(v'j') + Cl. ◆, translational energy; ◇, vibrational energy; ◆, rotational energy.

9. Vibrationally resolved angular differential cross section, $\sin^{-1}(\theta)\, d\sigma/d\theta$, versus center of mass angle, θ, at 8 km s^{-1} for the QCT-HB results for the transitions O + HCl(v=0,T=300) → OH(v') + Cl.

10. Total and electronic state component collisional excitation cross sections versus relative collision velocity for the QCT-HB results for the transition O + HCl(v=0,T=300) → HCl(v'=1) + Cl. ◆ ,total cross section; ◇, ^{3}A'' component; ◆, ^{3}A' component.

Appendix A. Figure Captions:

Figure A1. Fit of the O atom speed distribution showing the two Gaussian-like components and their sum from the measurements of Ref. 32. The maximum value is set to 1.0.

Figure A2. ----- $f_O(v)$, O-atom speed distribution distribution, Eq A1, times the speed squared, where the speed, v, for $f_O(v)$ refers to the O-atom speed in the NO_2 the center-of-mass frame; —— $f_{O\text{-}HCl}(v)$, relative O-HCl speed distribution from Eq. A2, where the speed, v, for $f_{O\text{-}HCl}(v)$ refers to the O-atom relative velocity in the O+HCl center-of-mass frame. Note that each distribution is normalized to unity.

Figure A3. O+HCl relative (normalized) translational energy distribution corresponding to the speed distribution, $f_{O\text{-}HCl}(v)$, shown in Figure A2.

FIGURE 1

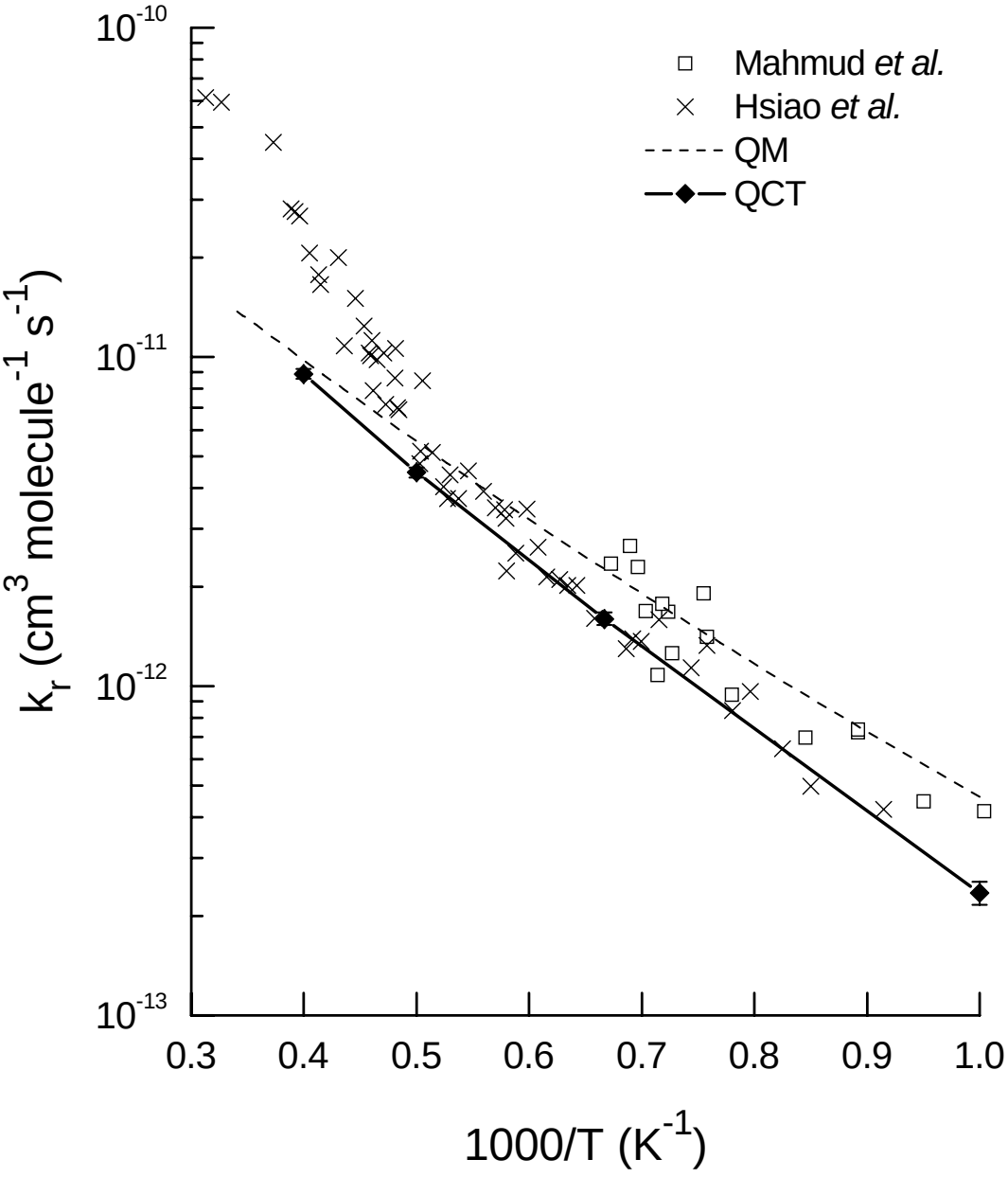
Mahmud *et al.*
Hsiao *et al.*
QM
QCT
10^{-10}
10^{-11}
10^{-12}
10^{-13}
k_r (cm^3 $molecule^{-1}$ s^{-1})
0.3
0.4
0.5
0.6
0.7
0.8
0.9
1.0
1000/T (K^{-1})

FIGURE 2

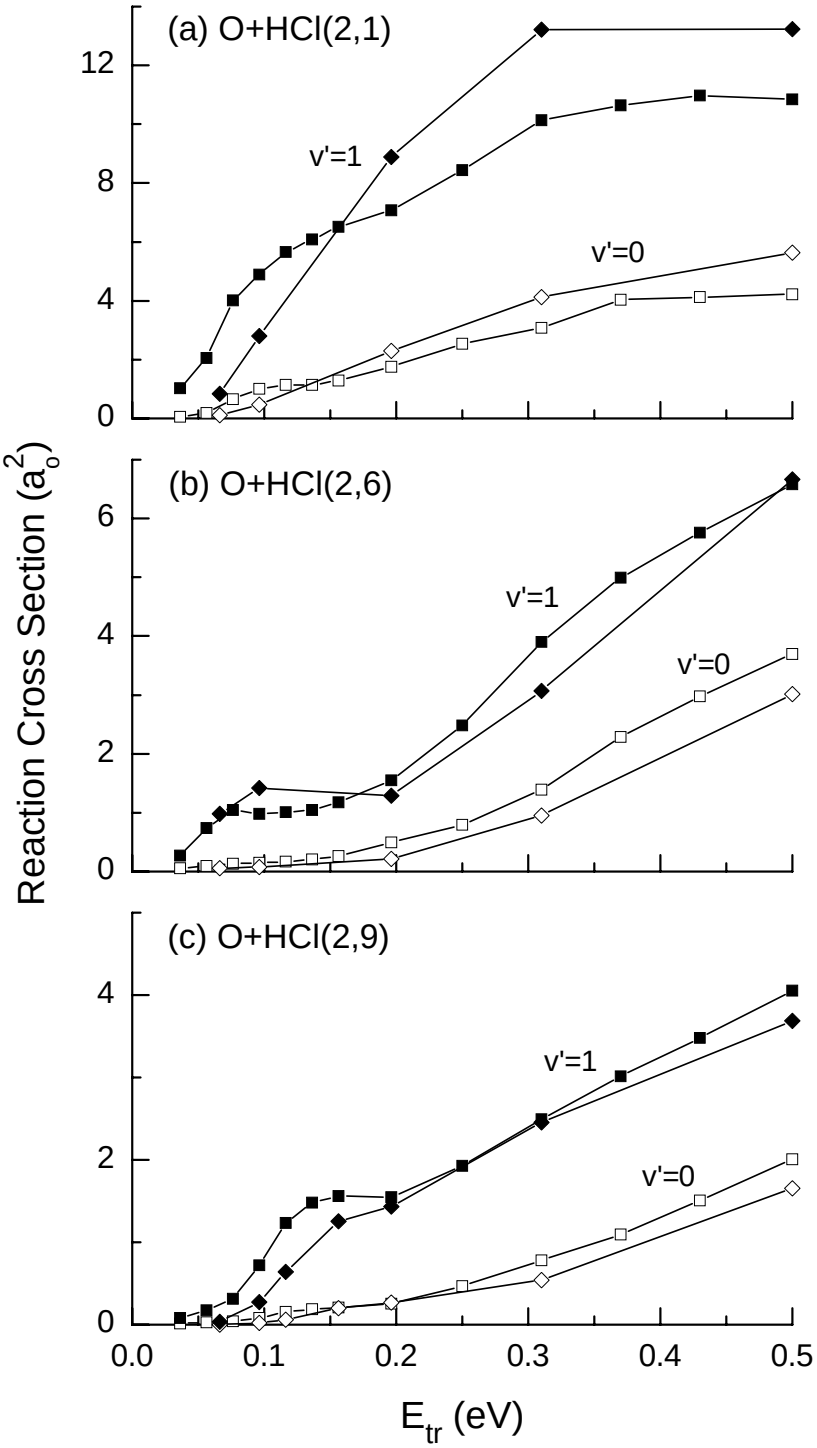
(a) O+HCl(2,1)
v'=1
v'=0
(b) O+HCl(2,6)
v'=1
v'=0
(c) O+HCl(2,9)
v'=1
v'=0
Reaction Cross Section (a_o^2)
E_{tr} (eV)
0
2
4
6
8
12
0.0
0.1
0.2
0.3
0.4
0.5

FIGURE 3

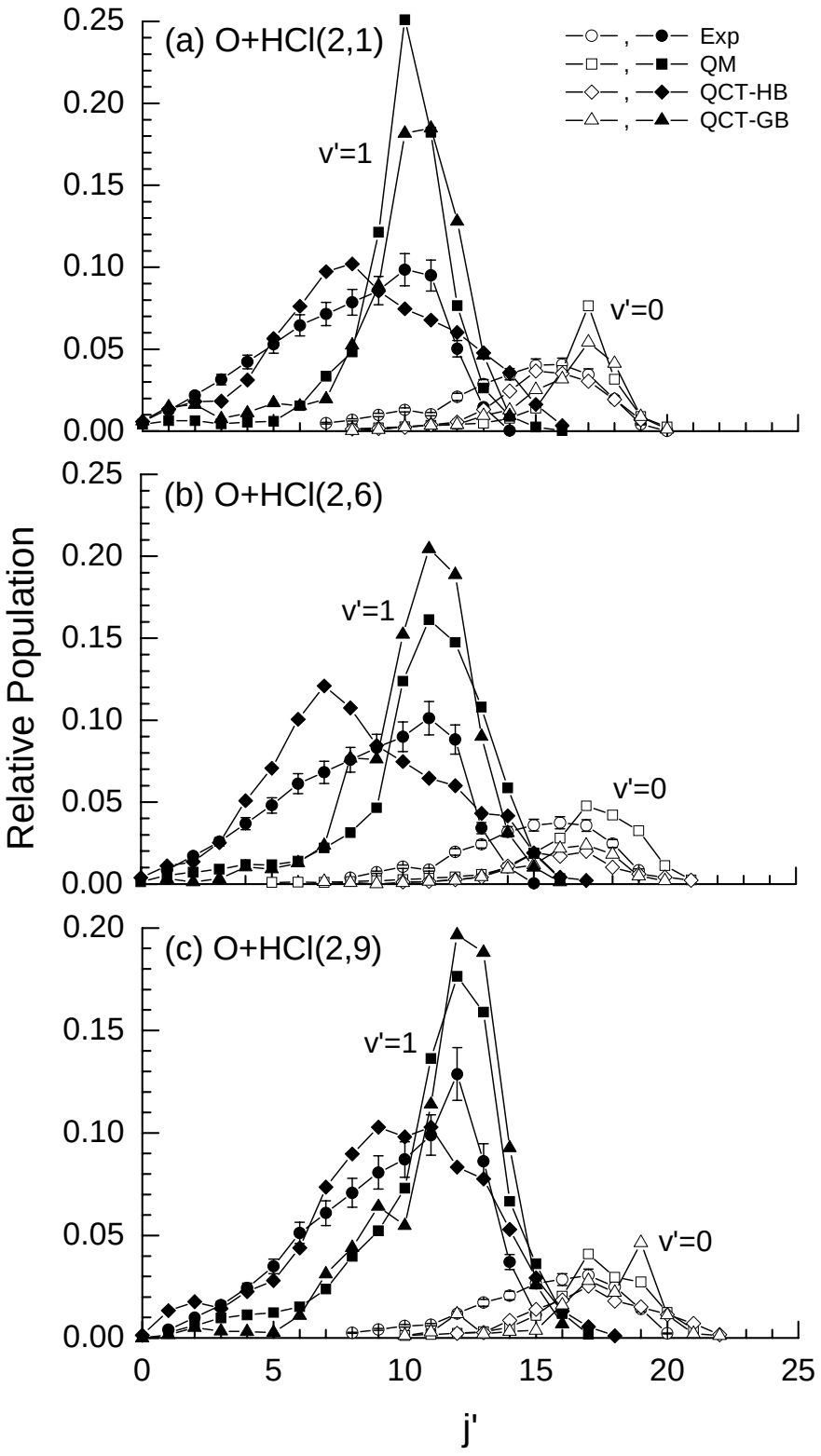
(a) O+HCl(2,1)
(b) O+HCl(2,6)
(c) O+HCl(2,9)
Exp
QM
QCT-HB
QCT-GB
v'=1
v'=0
Relative Population
j'
0.00
0.05
0.10
0.15
0.20
0.25
0
5
10
15
20
25

FIGURE 4

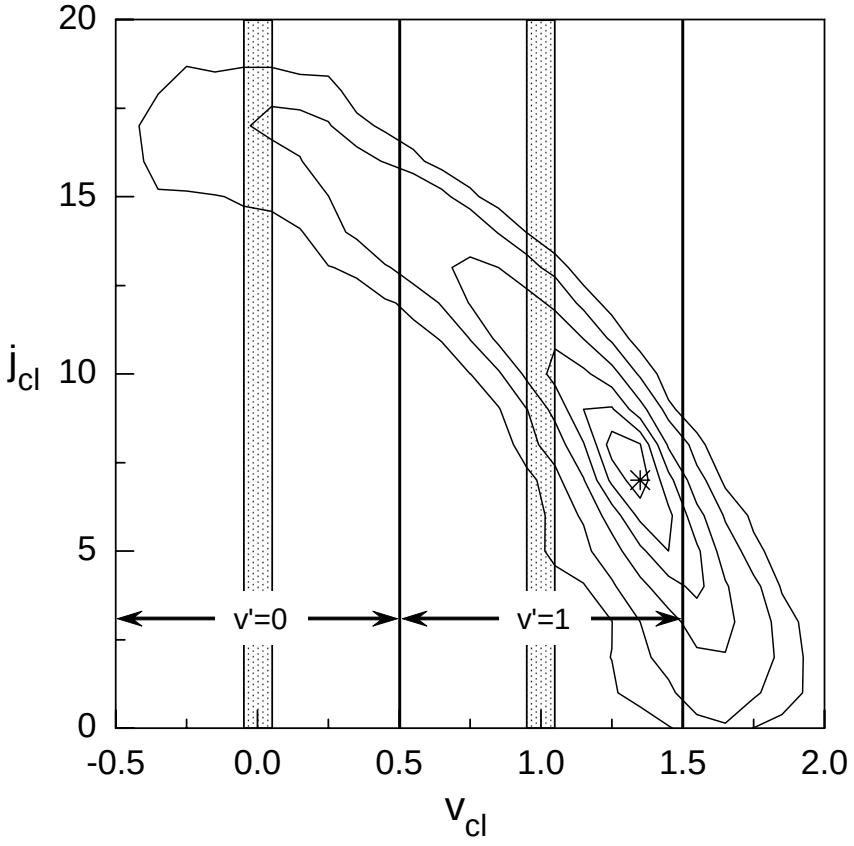

FIGURE 5

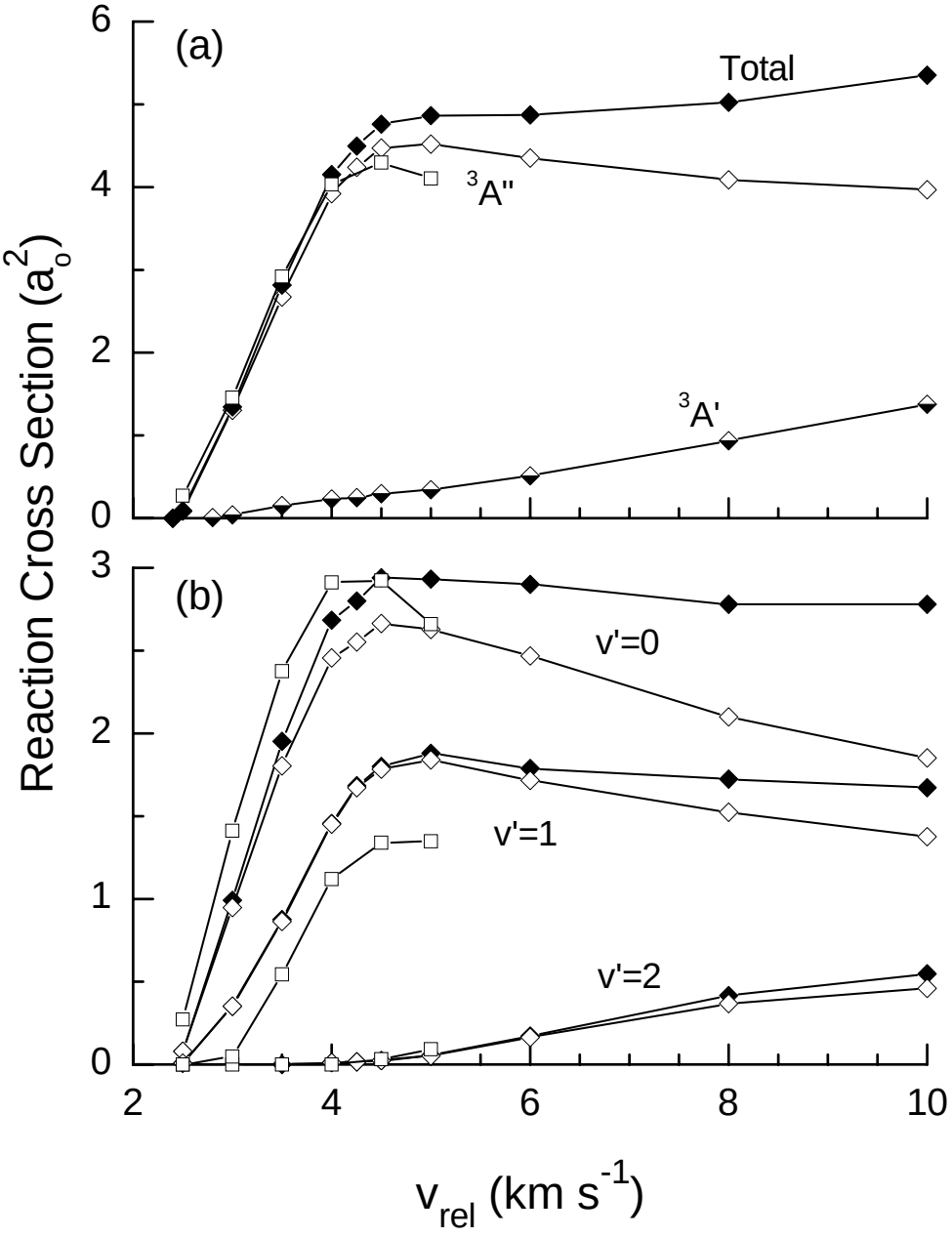
(a)
Total
^{3}A"
^{3}A'
(b)
v'=0
v'=1
v'=2
Reaction Cross Section (a_o^2)
v_{rel} (km s^{-1})
0
2
4
6
1
3
8
10

FIGURE 6

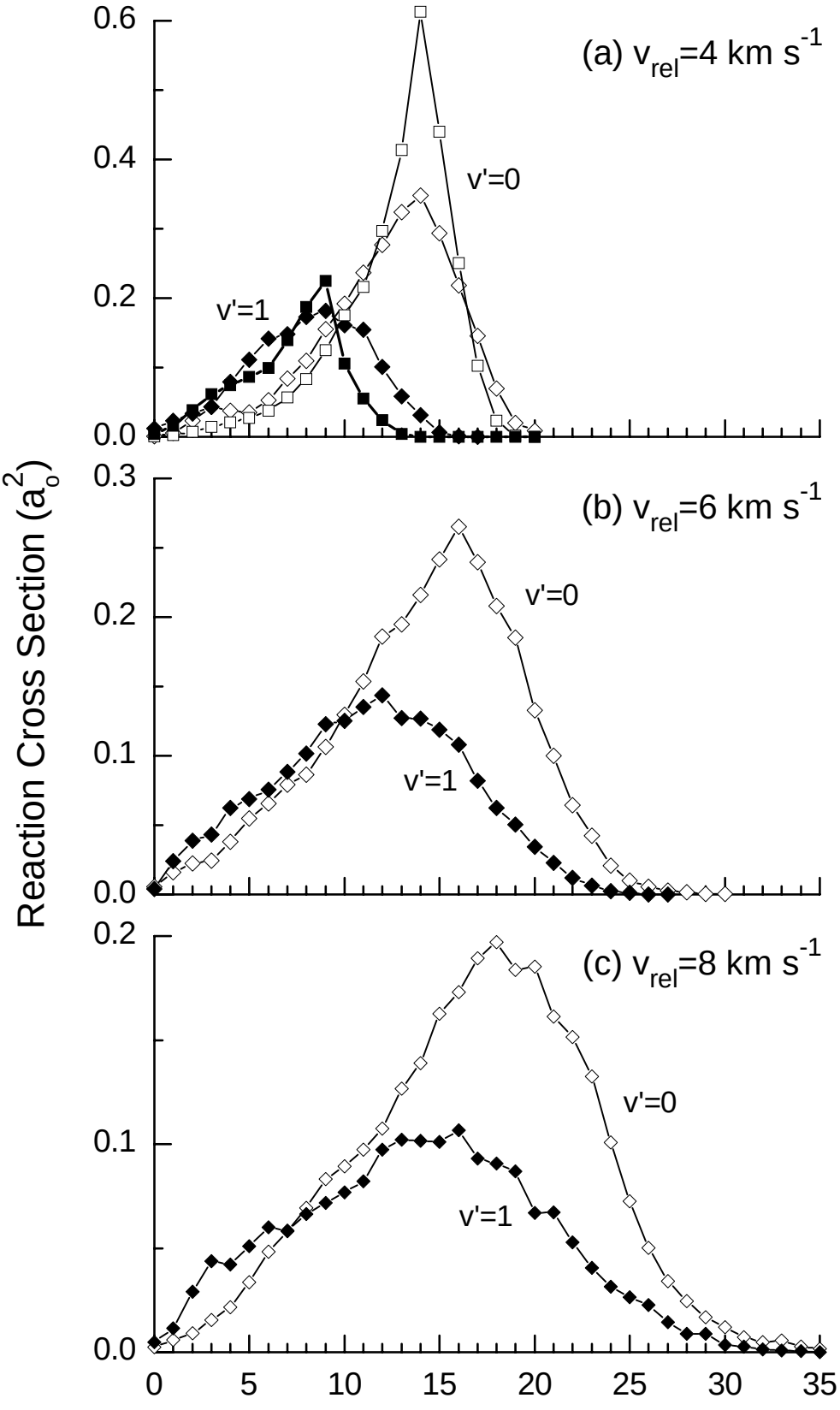
(a) v_{rel}=4 km s^{-1}
v'=0
v'=1
(b) v_{rel}=6 km s^{-1}
v'=0
v'=1
(c) v_{rel}=8 km s^{-1}
v'=0
v'=1
Reaction Cross Section (a_o^2)
j'
0.0
0.1
0.2
0.3
0.4
0.6
0
5
10
15
20
25
30
35

FIGURE 7

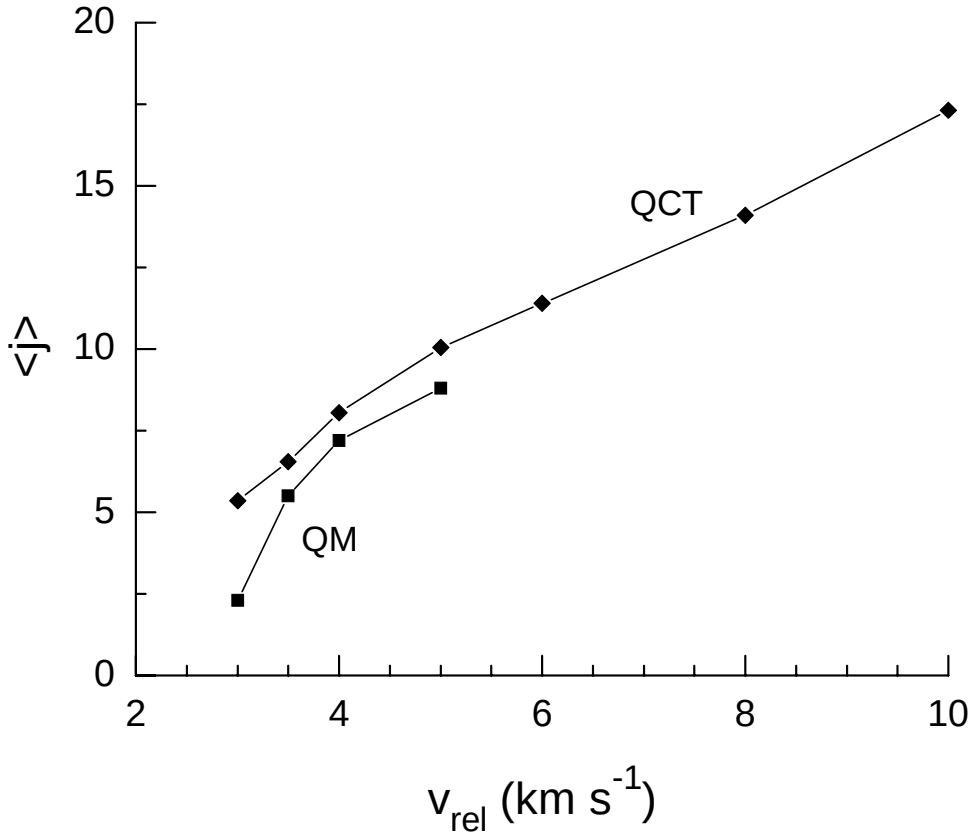

FIGURE 8

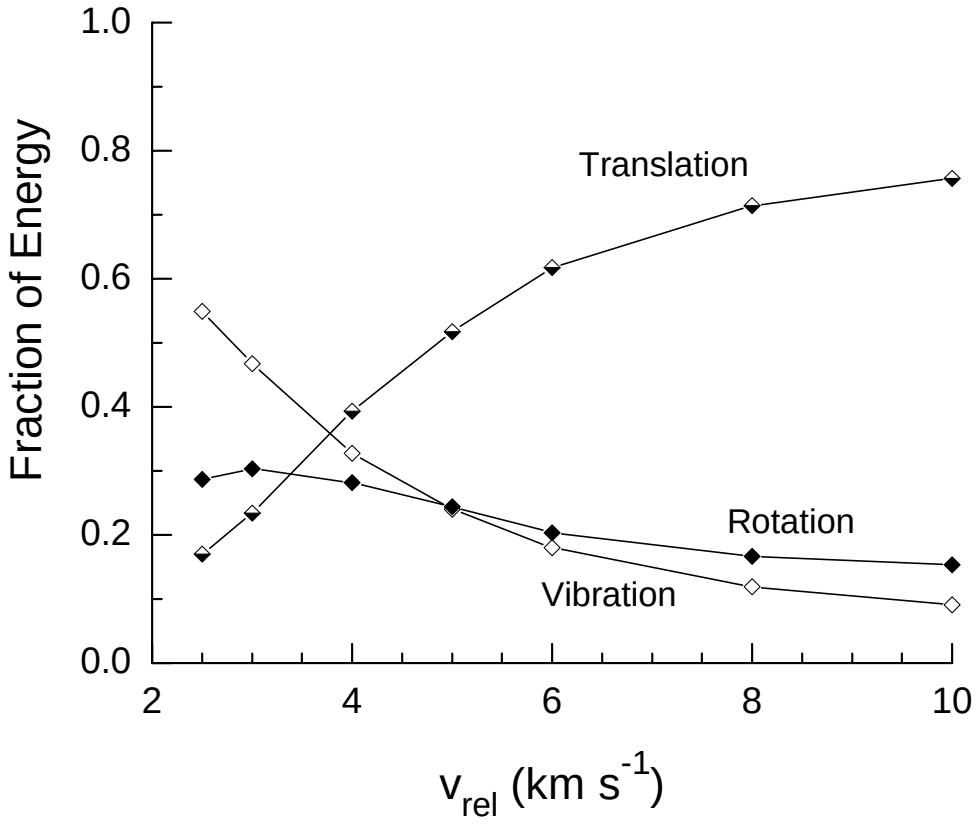
1.0
0.8
0.6
0.4
0.2
0.0
Fraction of Energy
Translation
Rotation
Vibration
2
4
6
8
10
v_{rel} (km s^{-1})

FIGURE 9

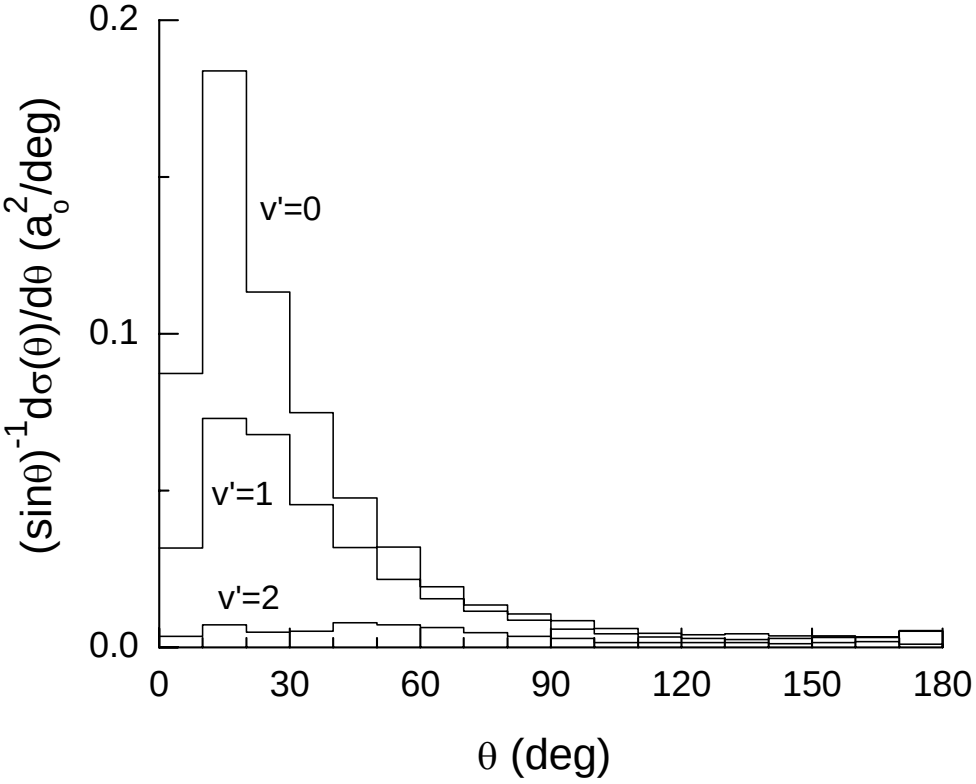

FIGURE 10

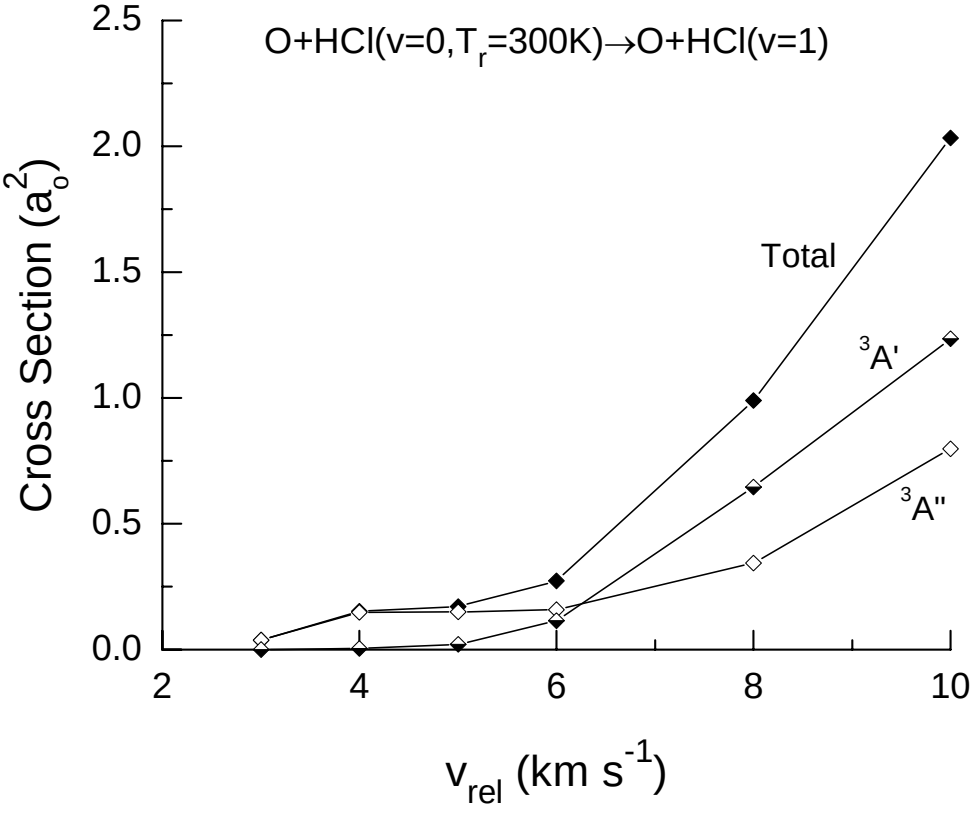
O+HCl(v=0,T$_r$=300K)→O+HCl(v=1)
Cross Section (a_o^2)
v_{rel} (km s^{-1})
Total
^{3}A'
^{3}A"
0.0
0.5
1.0
1.5
2.0
2.5
2
4
6
8
10

FIGURE A-1

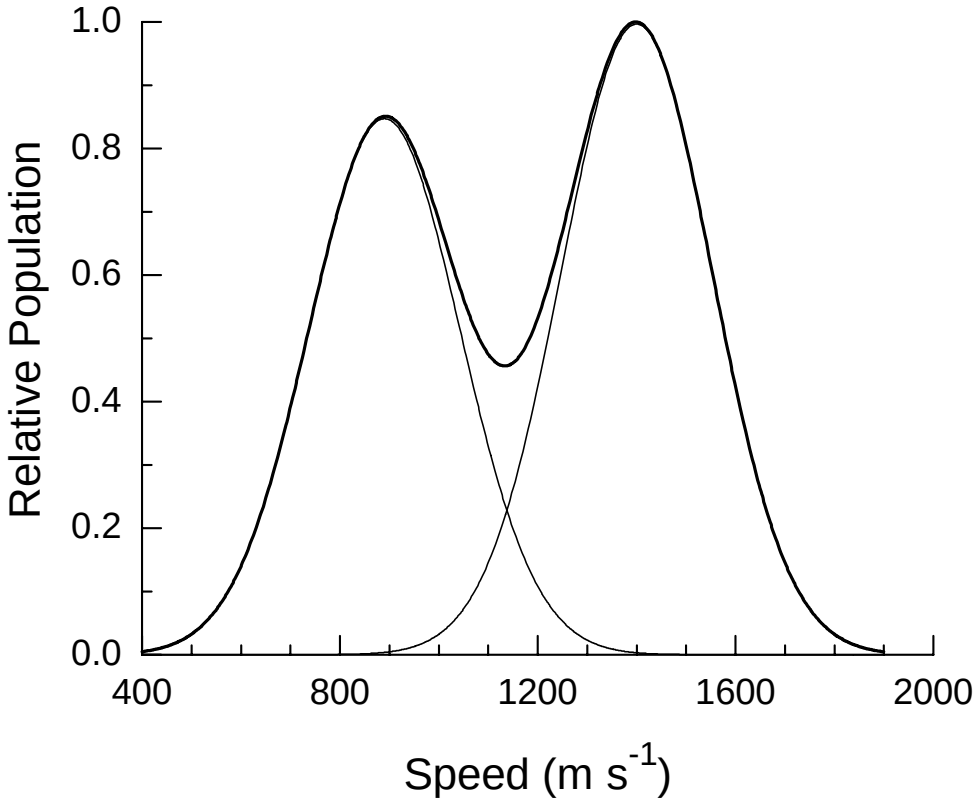
1.0
0.8
0.6
0.4
0.2
0.0
Relative Population
400
800
1200
1600
2000
Speed (m s-1)

FIGURE A-2

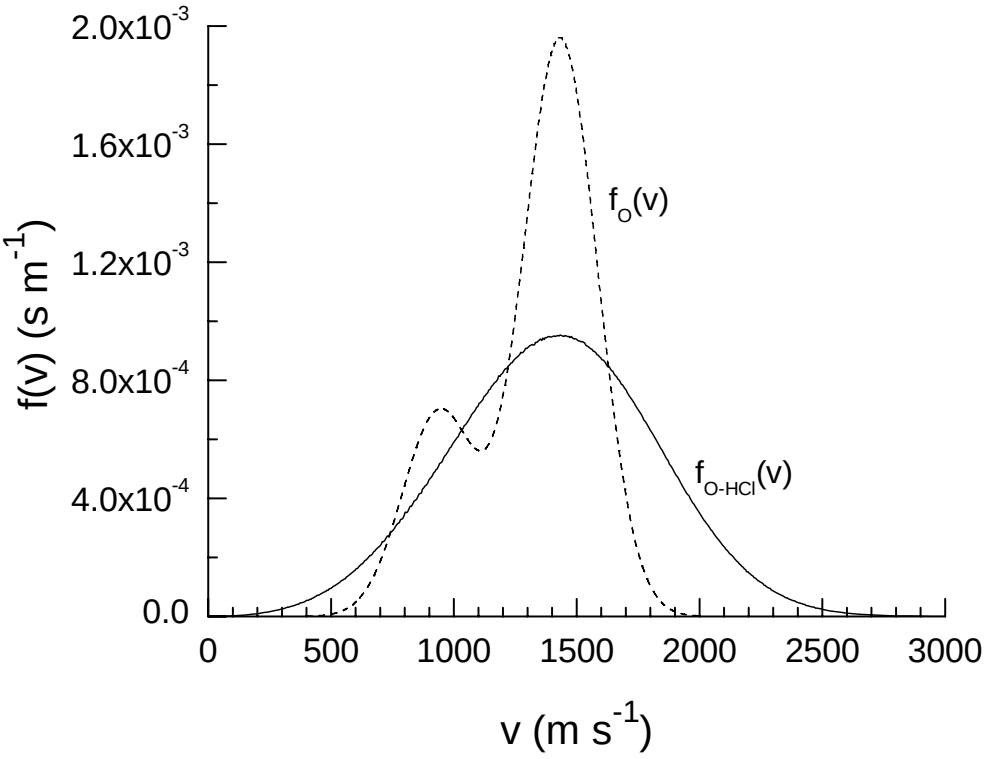
2.0x10-3
1.6x10-3
1.2x10-3
8.0x10-4
4.0x10-4
0.0
f(v) (s m-1)
fO(v)
fO-HCl(v)
0
500
1000
1500
2000
2500
3000
v (m s-1)

FIGURE A-3